The improved reconstruction of fluorescence molecular tomography via regularized doubly orthogonal matching pursuit method

Kong, Lingxin, An, Yu, Du, Yang, Tian, Jie

Lingxin Kong, Yu An, Yang Du, Jie Tian, "The improved reconstruction of fluorescence molecular tomography via regularized doubly orthogonal matching pursuit method," Proc. SPIE 11313, Medical Imaging 2020: Image Processing, 113131Q (10 March 2020); doi: 10.1117/12.2549247

SPIE.

Event: SPIE Medical Imaging, 2020, Houston, Texas, United States

The Improved Reconstruction of Fluorescence Molecular Tomography via Regularized Doubly Orthogonal Matching Pursuit Method

Lingxin Kong[1,2], Yu An[1,2,3], Yang Du[*,1,2], Jie Tian[*,1,2,3,4]

1. CAS Key Laboratory of Molecular Imaging, the State Key Laboratory of Management and Control for Complex Systems, Institute of Automation, Chinese Academy of Sciences, Beijing, 100190, China
2. The University of Chinese Academy of Sciences, Beijing, 100080, China
3. Beijing Advanced Innovation Center for Big Data-Based Precision Medicine, School of Medicine, Beihang University, Beijing, 100191, China
4. Engineering Research Center of Molecular and Neuro Imaging of Ministry of Education, School of Life Science and Technology, Xidian University, Xi'an, Shaanxi, 710126, China

*Corresponding author, E-mail: tian@ieee.org, yang.du@ia.ac.cn

ABSTRACT

Fluorescence molecular tomography (FMT) is a promising multimodality-fused medical imaging technique, aiming at noninvasively and dynamically visualizing the interaction processes at the cellular and molecular level. However, due to the intricate correlation among columns in system matrix, the inverse problem of FMT faces high ill-posedness. In this work, we propose a novel regularized doubly orthogonal matching pursuit (RDOMP) method through synergistically integrating Gram-Schmidt (GS) orthogonalization with regularized orthogonal matching pursuit (ROMP) to decorrelate the elements in support set against remaining elements. Experiments based on the numerical mouse with double tumors and *in vivo* mouse were conducted to validate the enhancement of RDOMP with comparison to orthogonal matching pursuit (OMP), sparsity adaptive subspace pursuit (SASP), and ROMP contrast methods. The simulated experimental results demonstrated a better performance of RDOMP in terms of location accuracy, fluorescent yield reconstruction, relative sparsity, and morphological similarity, which highlighted the pruning capability of the introduced GS orthogonalization. And *in vivo* experimental results demonstrated the practical application of RDOMP on FMT reconstruction.

Keywords: fluorescence molecular tomography, regularized doubly orthogonal matching pursuit, inverse problem, compressed sensing.

I. INTRODUCTION

As an extension of Fluorescence Molecular Imaging (FMI), Fluorescence Molecular Tomography (FMT) is a more promising imaging technology that fuses the tumor-specific information from FMI with anatomical information from Computed Tomography (CT), to comprehensively and objectively assess the diseased areas through three-dimensional visualization [1, 2]. However, the FMT inverse problem, which is based on the measurement data on the surface of the imaged object to reconstruct the tumor distribution in the whole spatial domain, commonly faces high ill-posedness [3].

Typically, we reformulate the FMT inverse equation for numerical treatment to alleviate the high ill-posedness by including additional assumption known as regularization [4]. Tikhonov regularization, regarded as the typical standard optimization method with the merits of easy to solve and mitigating overfitting, is widely used in FMT inverse problem but presents the drawback of over-smoothness [5]. Although Gao *et al* have attempted to enhance the Tikhonov regularization effect by fusing the Gaussian weighted Laplacian prior, and have improved the reconstruction performance to some extent, over-smoothness is still inevitable [6]. In addition, some researchers proposed other regularization term based on the L_1-norm, to reconstruct the tumor distribution, according to the prior that tumors sparsely distribute in the biological tissue [7]. Notably, all L_1-norm based FMT solving methods can be approximately divided into two parts, viz., proximal gradient method and greedy algorithm. Proximal gradient method is used for non-differentiable optimal problem through variable splitting and proximity operator to solve the inverse problem, including fast iterated shrinkage method [8], split Bregman method [9], joint L_1-norm and L_2-norm regularization [10], and joint L_1 and total variation regularization [11]. However, proximal gradient methods generally face high computational problems and time-consuming, since the scale of FMT inverse problem commonly reaches tens of thousands of dimensions, which

Medical Imaging 2020: Image Processing, edited by Ivana Išgum, Bennett A. Landman,
Proc. of SPIE Vol. 11313, 113131Q · © 2020 SPIE · CCC
code: 1605-7422/20/$21 · doi: 10.1117/12.2549247

is greatly restricted in practical application. It is worth mentioning that greedy algorithm based on compressed sensing theory as an alternative can achieve highly accurate reconstruction with low computational complexity, due to the concept of selecting most correlated atom and avoiding differential [12]. Orthogonal matching pursuit (OMP) is a typical greedy algorithm based on compressed sensing, and achieves approximate tumor reconstruction in FMT inverse problem [13]. Apart from OMP, some researchers subsequently proposed regularized orthogonal matching pursuit (ROMP) to accelerate the atom selection procedure and enhance the rightness of atom selection [14]. Moreover, sparsity adaptive subspace pursuit (SASP) was proposed to adaptively adjust the sparsity and check the validness of the support set by backtracking [15]. However, greedy based algorithm commonly faces incorrectness of atom selection due to the high correlation of columns of system matrix, which greatly affects the reconstruction accuracy.

In this work, we propose a novel regularized doubly orthogonal matching pursuit (RDOMP) method for FMT inverse problem by introducing the Gram-Schmidt (GS) orthogonalization into the regularized orthogonal matching pursuit (ROMP) at each iteration to decorrelate the correlation among support set and the remaining elements. To test the applicability of RDOMP in terms of its ability to improve the correctness of atom selection, we conducted numerical simulation experiments based on digital mouse and *in vivo* experiments on tumor bearing mouse.

II. METHODS

FMT inverse problem: the inverse problem of FMT reconstruction can be formulated by a low-order approximated and simplified model from the complex integral-differential radiative transfer equation, known as diffusion equation (DE) and as shown in Eq. 1.

$$\begin{cases} \nabla\left[D_x(r)\Phi_x(r)\right]-\mu_{ax}(r)\Phi_x(r)=-\Theta\delta(r-r_l) \\ \nabla\left[D_m(r)\Phi_m(r)\right]-\mu_{am}(r)\Phi_m(r)=-\Phi_x(r)\eta\mu_{af}(r) \end{cases} \quad (r\in\Omega), \tag{1}$$
$$2D_{x,m}(r)\partial\Phi_{x,m}(r)/\partial\vec{n}(r)+q\Phi_{x,m}(r)=0 \qquad (r\in\partial\Omega),$$

Considering the irregular properties of biological tissue, tetrahedronal finite element discretization of each organ is utilized for calculating the approximate solutions of Eq.1. Hence, the complicated differential equation of Eq. 1 can be simply formulated in Eq. 2.

$$\begin{cases} K_x\Phi_x=S_x, \\ K_m\Phi_m=GX, \end{cases} \tag{2}$$

Where K_m is symmetrical and positive definite, Eq.2 can be reformulated into following matrix-form equation, as shown in Eq. 3.

$$AX=\Phi, \tag{3}$$

Where $\Phi\in\mathbb{R}^n$ is the measurement vector, $A=[f_1,...,f_d]\in\mathbb{R}^{n\times d}$ ($n<d$) is the matrix of the feature vector $f_i\in\mathbb{R}^n$, and X is the coefficients vector. Owing to the high ill-posedness of Eq. 3, directly solving the Eq. 3 will result in poor reconstruction performance. Based on the prior that tumors sparsely distribute in the imaged object when compared with the whole imaging domain, we utilized the L_1-norm as regularization term to guide the solution processes. The sparsity constraint based L_1-norm regularization can be presented as following Eq. 4.

$$\min_X E(X)=\frac{1}{2}\left\|AX-\Phi\right\|_2^2+\lambda\left\|X\right\|_1 \tag{4}$$

Where λ is the hyper parameter governing the regularization effect of L_1-norm. Here, the columns of system matrix A can be treated as a set of basis vectors or atoms, while x forms the coefficients corresponding to each atom. Thus, the sparse constraint optimal problem can be transformed to a dictionary-learning problem on the concept that choosing atoms as little as possible with non-zero value to restore x. And the atom selection procedures commonly based on the greedy idea that choosing the atom with maximal correlation to residual error vector of present iteration. After iteratively processing the atom selection and updating support set, we finally get the candidate set corresponding to non-zero value in x. RDOMP adopts the greedy algorithms aiming at recovering the fluorescent yield through an iterative approach as shown in Eq. 5.

$$\min\left\|X\right\|_1 \text{ subject to } AX=\Phi \tag{5}$$

RDOMP algorithm: after defining the objective function and restrictions, we propose the RDOMP reconstruction method based on the idea to select a better group of proper basis vector through GS orthogonal decorrelation of system matrix columns, and synergistically embed GS orthogonalization into ROMP to solve the L_1-norm problem. The processes and details of RDOMP are shown in Algorithm. 1.

Algorithm 1: regularized doubly orthogonal matching pursuit (RDOMP)

INPUT: system matrix $A \in \mathbb{R}^{m \times n}$, measurement vector Φ

Initialization: support set $S^0 = \varnothing$, residual error vector $r^0 = \Phi$, $Z^0 = \mathrm{A}$, sparsity K, precision $\varepsilon > 0$, iteration number $k = 0$, threshold η.

Iteration:

while $\left\| r^k \right\|_2 > \varepsilon$ or $k < K$ do:

(1) $k = k + 1$;

(2) normalization: $Z_{\{i\}}^{k-1} = Z_{\{i\}}^{k-1} / \left\| Z_{\{i\}}^{k-1} \right\|_2$ where $i \notin S^{t-1}$;

(3) calculate residual error correlation: $u = Z_{\{i\}}^{t-1^T} r^{t-1}$;

(4) regularize selected elements: $J_{reg} = \{i, u(i) \geq \eta u_{\max}, i \in J\}$;

(5) Update support set: $S^k = S^{k-1} \bigcup J_{reg}$;

(6) GS orthogonalization: $p^k = Z_{\{i\}}^{k-1^T} Z^{k-1}$, $Z^k = Z^{k-1} - p^k \otimes Z_{\{i\}}^{k-1}$ $(i \in J_{reg})$;

(7) Calculate temporary solution: $x = A_{S^k}^{+} \Phi$;

(8) Compute residual error vector: $r = \Phi - proj\left(\Phi, A_{S^k}\right) = \Phi - A_{S^k} A_{S^k}^{+} \Phi$;

End while

OUTPUT: the reconstructed results x of FMT inverse problems.

The novelty of RDOMP is the additional GS orthogonalization module, which inputs a set of finite, linearly independent vectors and outputs an orthogonal set that spans the same dimensional subspace [16]. Through synergistically integrating GS orthogonalization into ROMP, which greatly eliminates the impact of candidates in support set on system matrix to decorrelate the basis vectors of system matrix, and thus to alleviate the ill-posedness of system matrix and enhance the correctness of atom selection. It is noteworthy that GS orthogonalization operated on each newly added atom in support set. The details of GS orthogonalization are given in Eq. 6.

$$p^k = Z_{\{i\}}^{k-1^T} Z^{k-1}, \quad Z^k = Z^{k-1} - p^k \otimes Z_{\{i\}}^{k-1} \quad (i \in J_{reg}) \tag{6}$$

Where $p \in C^n$ is the projection vector of selected vector on each column of system matrix, and the operator $\otimes$ is the Kronecker product resulting in a block matrix in order to match the system matrix size. After each column of system matrix subtracts the projected vector, it is orthogonal to the remaining basis set from the selected components to reduce the impact of selected components in J_{reg} on remaining candidates.

***Evaluation index*:** in this work, we use position error (PE), reconstructed fluorescent yield (RFY), percentage of non-zero components (PNZ), and the Dice coefficient to quantitatively assess the reconstruction performance [17].

$$PE = \left\| P_r - P_0 \right\|_2, \quad RFY = \frac{\sum X_{NOI}}{N_{NOI}}, \quad PNZ = \frac{N_{NOI}}{N}, \quad Dice = \frac{2\left|X \cap Y\right|}{\left|X\right| + \left|Y\right|}, \tag{7}$$

Where P_r and P_0 represent the reconstructed tumor centers and ground truth center respectively, NOI indicates the nodes of interests, X_{NOI} represents fluorescent yield of each node in NOI, N_{NOI} is the number of nodes in NOI, X is the reconstructed region and Y is the ground truth region. All indicators except PE are the greater, the better the reconstruction performance, with one as the upper limitation; while the PE is the smaller, the better locating performance, with the zero as thelower limitation .

III. EXPERIMENTS AND RESULTS

In order to comprehensively evaluate the reconstruction performance of RDOMP in terms of accuracy, and practicability, numerical simulation experiments and *in vivo* mouse experiment were implemented in this section. Contrast methods including OMP, SASP, and ROMP were utilized for comparison. All the computational processes were conducted on a desktop computer equipped with a 3.4GHz i7-6700 CPU, a Nvidia 1080Ti GPU, and 16GB RAM.

As for the configuration of FMT forward problem in numerical experiment, we implemented homogeneous truncated digital mouse atlas with artificially added tumors inside liver to form numerical simulation [18]. And based on the finite-element theory, we discretized the segmented biological tissues viz., bone, heart, liver, kidney, lung, and muscle into

meshes. Subsequently, we utilized the optical parameters as same excitation and emission light wavelength as *in vivo* experiment to formulate the system matrix, which was shown in Table. I. To collect as much information as possible, the excitation and emission processes were repeated at four different angles around the imaged object. Finally, we calculated the forward problem of FMT to get the measurement data and assembled the four angles measurement data with its corresponding system matrix based on forward mesh with 15639 nodes and 84507 elements, as shown in Fig. 1.

TABLE I

OPTICAL ABSORPTION AND SCATTERING COEFFICIENTS OF BIOLOGICAL TISSUES IN NUMERICAL AND IN VIVO EXPERIMENTS

Tissue	μ_{ax}	μ_{am}	μ'_{sx}	μ'_{sm}	G
Bone	0.0521	0.0326	2.4415	2.114	0.93
Heart	0.0504	0.0331	0.9437	0.8203	0.9
Liver	0.3016	0.1921	0.6676	0.6023	0.93
Kidney	0.0566	0.0377	2.2032	1.9002	0.9
Lung	0.1681	0.1045	2.1569	2.0477	0.93
Muscle	0.0745	0.0474	0.4115	0.3122	0.97

Units of μ_a and μ'_s: mm−1

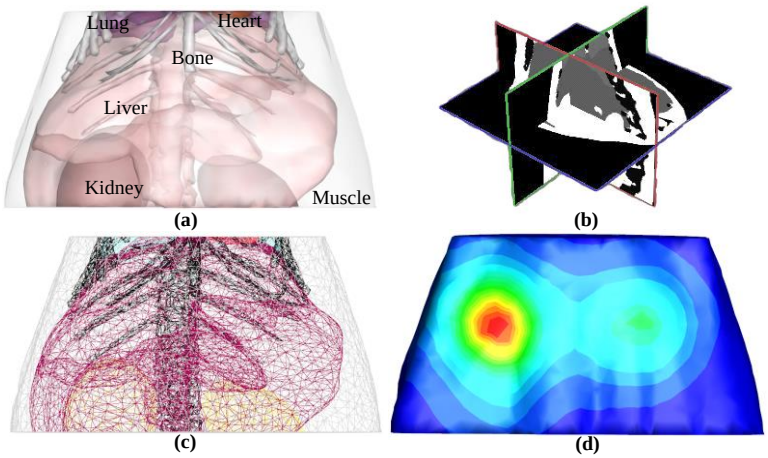

Fig. 1 The visualization of homogeneous truncated digital mouse. (a) Distribution of biological tissues; (b) orthogonal slice view; (c) discretized mesh; (d) surface spotlight.

Because photon propagation in real conditions does not depend on discretized forward mesh, which only used to approximate measurement data through light transmission among biological tissue, thus, we adopted another mesh with 15175 nodes, 82857 elements in inverse problem. In simulation experiments, we set up two spherical tumors inside liver with center coordinates of (6.5, 12.7, 7.5) and (6.5, 21.7, 7.5). Both radii were set to 0.8 mm and fluorescent yield were set to 1 mm^{-1}. The hyper parameters of RDOMP K, ε, η were emperically set to 10, 0.05×norm(Φ), 0.5 respectively. And OMP, SASP, and ROMP were implememted as contrast experiments with same hyperparameters K and ε.

The qualitative analysis is shown in Fig. 2 (a-d) consisting of 3D view of the whole imaged object and slice view of tumor located plane. It was worth noting that though all methods can approximately reconstruct the tumor region, RDOMP still achieved higher morphological similarity and lower location error, since more overlapped area between ground truth and reconstructed region. Besides, comparison methods such as SASP and ROMP faced reconstruction problems that small discontinuous tumors located near ground truth region, while RDOMP was not troubled by this problem. Furthermore, a series of evaluating indexes were utilized to quantitatively assess the reconstruction performance. As shown in Fig. 2 (e), it can be seen that RDOMP achieved lower PE, much higher Dice and PNZ, while RFY was almost at the similar level, when compared to OMP, SASP, and ROMP. Thus, quantitative analysis demonstrated the better performance of RDOMP in locating tumors, sparsely reconstruction, and morphological similarity. It can be concluded from numerical experiments that the addition of GS module plays a critical role through enabling the selection of a better set of components by decorrelating the highly correlated columns of system matrix.

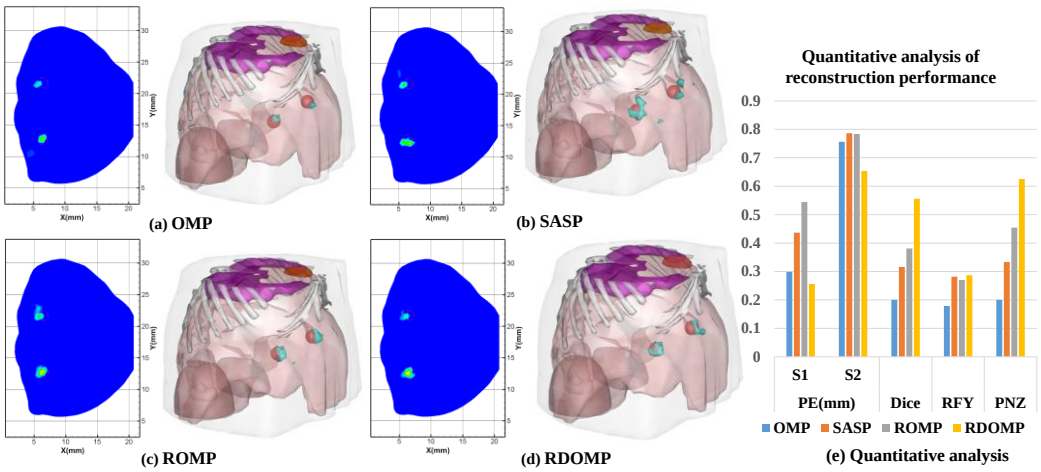

Fig. 2 The qualitative and quantitative analysis of OMP, SASP, ROMP, and RDOMP reconstruction performance. The red dotted circles in (a)-(d) represent the real fluorescent sources. It is assumed that the green polygons clustered around the red spheres in the 3D view are reconstructed tumors; (e) quantitative analysis results.

Furthermore, we implemented the *in vivo* liver tumor-bearing mouse experiments to validate reconstruction performance on real condition based on multimodality-fused imaging system to acquire FMI, CT, and MRI images [19]. The hybrid system was equipped with a continuous wave laser for excitation, an ultrasensitive EMCCD camera with a 160° field of view (FOV) to acquire the fluorescent information, a micro-CT consisting of X-ray tube and detector to collect structural information, and a MRI device. It was worth noting that MRI images were used as ground truth due to the high contrast imaging ability of soft tissues to detect the tumor region. Different from numerical experiments, the *in vivo* experiments are more complex which required the procedures of data acquisition, signal denoising, organ segmentation and integration, imaged object discretizing and meshing, and 3D-2D mapping, step by step.

The reconstructed results in Fig. 3 demonstrated the better performance of RDOMP on locating the tumor center and reconstructing the tumor region without region splitting or false negative regions. However, contrast methods suffer those problems and have difficulties in identifying tumor number and region. Those improvements demonstrated the utilization of GS orthogonalization contributed to more correctly select residual error related atom, and thus enhanced the reconstruction performance. In general, *in vivo* experiment potentially highlighted the pre-clinical application of RDOMP on FMT reconstruction.

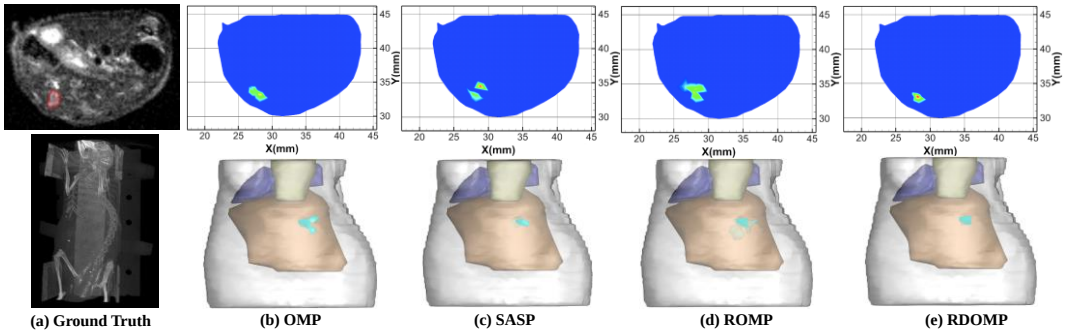

Fig. 3 *in vivo* reconstruction result in 3D view and sectional view by the proposed and comparison method. Pink region in (a) represents the tumor region.

IV. CONCLUSION

In this work, a novel FMT reconstruction method, RDOMP, was proposed by incorporating the GS orthogonalization with the ROMP. The motivation behind the proposed method is that the GS orthogonalization can decorrelate the complicated correlation among columns of system matrix by eliminating the impact of candidates in support set on system matrix, which enables the selection of a better set of components, and hence alleviate the ill-posedness of the

FMT inverse problem. Simulation experiments demonstrated the enhanced performance on reconstruction accuracy, morphological similarity, restored fluorescent yield, and relative sparsity of RDOMP than OMP, SASP and ROMP. And *in vivo* experiments also demonstrated the better reconstruction performance, which potentially addressed the practical application of RDOMP on FMT reconstruction. In general, RDOMP provides a new idea for the improvement of FMT reconstruction that alleviation of the ill-posedness by decorrelating the columns of system matrix is also a feasible and effective approach to enhance the performance other than adding regularization terms.

V. ACKNOWLEDGEMENTS

This work was supported by Ministry of Science and Technology of China under Grant No. 2017YFA0205; National Natural Science Foundation of China under Grant No. 81871514, 81227901, 81470083, 91859119, 61671449, 81527805; National Public Welfare Basic Scientific Research Program of Chinese Academy of Medical Sciences under Grant No. 2018PT32003, 2017PT32004, National Key R&D Program of China under Grant No. 2018YFC0910602, 2017YFA0205200, 2017YFA0700401, 2016YFA0100902, 2016YFC0103702; General Financial Grant from the China Postdoctoral Science Foundation under Grant No. 2017M620952.

VI. REFERENCE

[1] A. Ale *et al.*, "FMT-XCT: in vivo animal studies with hybrid fluorescence molecular tomography–X-ray computed tomography," *Nature methods,* vol. 9, no. 6, pp. 615, 2012.

[2] M. Koch *et al.*, "Tackling standardization in fluorescence molecular imaging," *Nature Photonics,* vol. 12, no. 9, pp. 505-515, 2018.

[3] Y. An *et al.*, "A novel region reconstruction method for fluorescence molecular tomography," *IEEE Transactions on biomedical engineering,* vol. 62, no. 7, pp. 1818-1826, 2015.

[4] Y. An *et al.*, "Recent methodology advances in fluorescence molecular tomography," *Visual Computing for Industry, Biomedicine, and Art,* vol. 1, no. 1, pp. 1, 2018.

[5] Y. Zhou *et al.*, "Self-prior strategy for organ reconstruction in fluorescence molecular tomography," *Biomedical optics express,* vol. 8, no. 10, pp. 4671-4686, 2017.

[6] Y. Gao *et al.*, "Bioluminescence Tomography Based on Gaussian Weighted Laplace Prior Regularization for In Vivo Morphological Imaging of Glioma," *IEEE transactions on medical imaging,* vol. 36, no. 11, pp. 2343-2354, 2017.

[7] D. Han *et al.*, "Sparsity-promoting tomographic fluorescence imaging with simplified spherical harmonics approximation," *IEEE Transactions on Biomedical Engineering,* vol. 57, no. 10, pp. 2564-2567, 2010.

[8] D. Han *et al.*, "A fast reconstruction algorithm for fluorescence molecular tomography with sparsity regularization," *Optics express,* vol. 18, no. 8, pp. 8630-8646, 2010.

[9] C. Leng *et al.*, "Reconstruction method for optical tomography based on the linearized Bregman iteration with sparse regularization," *Computational and mathematical methods in medicine,* vol. 2015, 2015.

[10] S. Jiang *et al.*, "Novel l 2, 1-norm optimization method for fluorescence molecular tomography reconstruction," *Biomedical optics express,* vol. 7, no. 6, pp. 2342-2359, 2016.

[11] J. Dutta *et al.*, "Joint L1 and total variation regularization for fluorescence molecular tomography," *Physics in Medicine & Biology,* vol. 57, no. 6, pp. 1459, 2012.

[12] M. Cai *et al.*, "Robust sparse reconstruction for Cherenkov luminescence tomography based on look ahead orthogonal matching pursuit algorithm." p. 1087114.

[13] J. A. Tropp *et al.*, "Signal recovery from random measurements via orthogonal matching pursuit," *IEEE Transactions on information theory,* vol. 53, no. 12, pp. 4655-4666, 2007.

[14] V. Michel *et al.*, "The regularized orthogonal functional matching pursuit for ill-posed inverse problems," *SIAM Journal on Numerical Analysis,* vol. 54, no. 1, pp. 262-287, 2016.

[15] J. Ye *et al.*, "Fast and robust reconstruction for fluorescence molecular tomography via a sparsity adaptive subspace pursuit method," *Biomedical optics express,* vol. 5, no. 2, pp. 387-406, 2014.

[16] D. Wang *et al.*, "Unsupervised feature selection through Gram–Schmidt orthogonalization—A word co-occurrence perspective," *Neurocomputing,* vol. 173, pp. 845-854, 2016.

[17] X. He *et al.*, "Half Thresholding Pursuit Algorithm for Fluorescence Molecular Tomography," *IEEE Transactions on Biomedical Engineering,* vol. 66, no. 5, pp. 1468-1476, 2018.

[18] D. Belma *et al.*, "Digimouse: a 3D whole body mouse atlas from CT and cryosection data," *Physics in Medicine & Biology,* vol. 52, no. 3, pp. 577-587, 2007.

[19] C. Chi *et al.*, "In vivo pentamodal tomographic imaging for small animals," *Biomedical Optics Express,* vol. 8, no. 3, pp. 1356-1371, 2017.